A primer to scaffolded DNA origami

Carlos Ernesto Castro[1], Fabian Kilchherr[1], Do-Nyun Kim[2], Enrique Lin Shiao[1], Tobias Wauer[1], Philipp Wortmann[1], Mark Bathe[2] & Hendrik Dietz[1]

Molecular self-assembly with scaffolded DNA origami enables building custom-shaped nanometer-scale objects with molecular weights in the megadalton regime. Here we provide a practical guide for design and assembly of scaffolded DNA origami objects. We also introduce a computational tool for predicting the structure of DNA origami objects and provide information on the conditions under which DNA origami objects can be expected to maintain their structure.

Scaffolded DNA origami allows the arrangement of thousands of nucleotides with sub-nanometer precision at specified locations in space to yield a diversity of objects with nanometer-scale dimensions[1–19] (**Fig. 1**). DNA origami entails folding a single-stranded 'scaffold' DNA molecule up to several thousand bases long into close-packed bundles of B-form DNA double-helical domains with single-stranded 'staple' oligonucleotides. The basic volume element in DNA origami is a Watson-Crick base pair stacked into double-helical DNA domains of defined length. DNA origami objects can be designed with custom software[4,9] and the manual labor required for assembly and purification is limited to handling pipettes and running agarose gels. Comprehensive reviews on the evolution and perspective of DNA origami have recently been published[20,21].

Applications are emerging that take advantage of the control over nanoscale shape afforded by DNA origami. Detergent-resistant 800-nm-long DNA nanotubes serve as liquid-crystalline alignment medium for the structural analysis of membrane proteins by nuclear magnetic resonance[3]. Functionalized DNA origami objects for various applications can be created by integrating staple oligonucleotides carrying functional groups such as fluorescent dyes or chemical groups that serve as anchors for the site-directed attachment of proteins, quantum dots and other nanoparticles. Various elegant anchoring strategies have been established[19,22–30]. Functionalized DNA origami objects have been used as calibration standards for super-resolution fluorescence microscopes[31], for the single-molecule study of chemical reactions[32] and for templating carbon nanotube–based transistors[33].

Here we provide a practical guide to building objects using scaffold DNA origami. We discuss DNA origami design rules, introduce a computational framework for predicting the structure of DNA origami objects to facilitate design and present conditions under which DNA origami shapes may be expected to remain structurally intact. Finally, we describe the workflow for design, production and quality control of DNA origami objects.

DNA origami object design

Designing a DNA origami object can be likened to developing a blueprint for a building. The location and shape of each brick forming part of the building needs to be specified. In scaffolded DNA origami, the bricks are double-helical DNA domains formed by a set of short single-stranded staple oligonucleotides that hybridize to a long single-stranded scaffold molecule. The scaffold sequence serves as an input to determine the sequences of the staple strands. Open-source DNA origami design software called caDNAno can facilitate designing DNA origami objects (http://cadnano.org/)[9].

The DNA origami design concept is illustrated in **Figure 2**. In DNA origami objects, double-helical domains are connected to adjacent double-helical domains by multiple interhelix connections consisting of immobilized Holliday junctions[34]. The interhelix connections are typically formed by antiparallel cross-overs[35,36] of either the staple or scaffold strand from one DNA double-helical domain to a neighboring one (**Fig. 2b**).

Double-helical domains tend to bow out between cross-overs owing to effects such as electrostatic repulsion and/or detailed geometry of cross-overs[1] (**Fig. 2b**). The extent of the bowing out depends on the distance between consecutive cross-overs[1]. In single-layer DNA origami objects, the bowing out creates an interhelical domain gap up to 1.5 nm when using a cross-over density of one cross-over every 26 base pairs (bp), whereas with a cross-over density of one cross-over every 16 bp, the gap

[1]Center for Integrated Protein Science Munich, Physics Department and Walter Schottky Institut, Technische Universität München, Garching, Germany. [2]Department of Biological Engineering, Massachusetts Institute of Technology, Cambridge, Massachusetts, USA. Correspondence should be addressed to H.D. (dietz@tum.de).

Figure 1 | Examples of objects built with scaffolded DNA origami. (**a**) Designs of single-layer DNA origami shapes (top) and AFM images of these objects (middle and bottom). The pointed star and the smiley face each have diameters of ~100 nm. Reprinted from ref. 1. (**b**) AFM image of crystalline DNA origami arrays formed from several hundred copies of a cross-shaped single-layer DNA origami object. Inset, image of a 100-nm-long cross-shaped origami monomer. Reprinted from ref. 18. (**c**) Container-like DNA origami objects (left) imaged with negative-stain TEM (top) and cryogenic TEM (bottom); reprinted from ref. 5 (top) and ref. 6 (bottom). (**d**) Design and images of multilayer DNA origami objects[7]. (**e**) Image of a multimeric multilayer DNA origami object with global twist deformation[8]. (**f,g**) Design and images of space-filling multilayer DNA origami objects such as bent bars (**f**) and a gear with square teeth (**g**) displaying custom curvature[8]. (**h**) Tensegrity prism created by combining multilayer DNA origami struts and ssDNA strings; reprinted from ref. 16. (**i**) Design and image of a single-layer DNA origami shape with site-directed protein attachments; reprinted from ref. 19. Scale bars, 100 nm (**a**), 1,000 nm (**b**) and 20 nm (**c–i**).
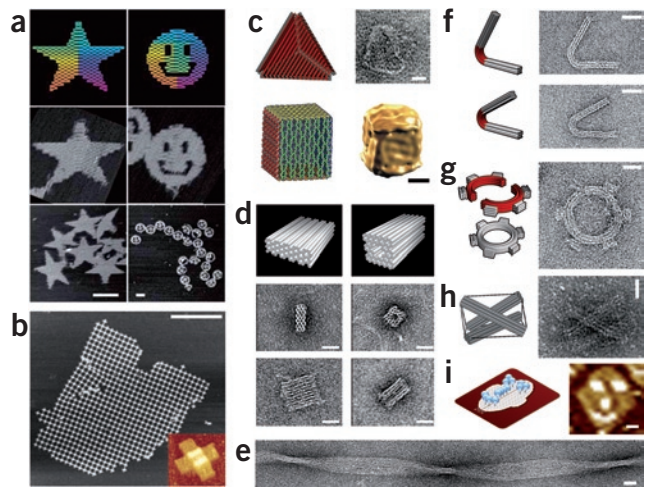
shrinks to 1 nm (ref. 1). In multilayer DNA origami structures with high cross-over densities of one every 7 bp or 8 bp, the interhelical gap appears smaller than 0.5 nm (refs. 7,10). The density of cross-overs impacts the effective dimensions of DNA origami objects.

One of the two strands in the double-helical domains in a DNA origami object is formed by a segment of a continuous single-stranded scaffold DNA molecule that runs through the entire object[1]. A first step in designing a DNA origami object is to route the scaffold through all DNA double-helical domains that make up the object. If using a circular scaffold, the routing must end where it begins. Scaffold DNA strands can also be prepared in linearized form. Possible solutions for routing a circular scaffold strand through two objects consisting of single layers of double-helical domains and through a multilayer object are illustrated in **Figure 2c**.

The strands complementary to the scaffold strand in double-helical domains are formed by single-stranded staple DNA oligonucleotides. Staples typically supply the majority of cross-overs that connect adjacent double-helical domains in DNA origami objects. Staple cross-overs may be assigned between adjacent double-helical domains at all positions where the staple backbone orientations of the neighboring double-helical domains coincide. Individual staples must be linear because forming double-helical domains with the scaffold requires free ends. Staples can undergo multiple cross-overs and thus connect multiple double-helical domains, but they must obey length constraints that we will discuss. Adding staples to the previously prepared scaffold routing results in a combined scaffold-staple layout (**Fig. 2d,e**).

For the sake of clarity in the case of multilayer objects, one can project the three-dimensional (3D) multilayer scaffold-staple layout onto a two-dimensional diagram in which each layer is treated separately. The need for displaying interhelix cross-overs between layers adds apparent complexity to these diagrams (example diagrams for multilayer objects are available in **Supplementary Figs. 1–5**). The DNA origami design software caDNAno[9] enables convenient editing of such two-dimensional diagrams for single-layer and multilayer objects (**Supplementary Note 1**).

DNA origami objects may also include single-stranded domains in addition to double-helical domains. This can be achieved by leaving segments of the scaffold strand unpaired or by adding segments to staple paths that do not bind to the scaffold. Single-stranded scaffold segments can be used as entropic springs to support tensegrity

structures[16], and they are useful in preventing unwanted base-stacking interactions at object interfaces[1,7]. Both single-stranded scaffold or staple segments may also serve as hybridization anchors for site-directed attachments.

Parsing the scaffold routing scheme with an input scaffold sequence determines the output sequences for the staples as defined in the scaffold-staple layout. There is not necessarily a unique set of staples that make the design. When using circular scaffolds, cyclic permutations of the scaffold strand sequence can generate multiple working sets of staple sequences. Particular permutations may be picked based on criteria such as where to place specific scaffold sequence motifs in the object. To determine staple sequences, the scaffold-staple layout can be parsed with an input scaffold sequence string by hand (very tedious), by *ad hoc* computer programs (less tedious) or with caDNAno, which accomplishes this feat upon a single mouse 'click'[9].

DNA origami packing and cross-over spacing rules

For building container-like objects using DNA origami, one may fold up single layers of helices (**Fig. 1c**)[5,6,13]. For space-filling shapes one may adopt a multilayer approach (**Fig. 1d–h**)[7,8,10,16]. Single-layer objects assemble with nearly 100% yield within a few hours[1]. The assembly of multilayer objects may take up to a week, and the yield of assembly depends on their structure and may be 5–20%[7]. Salt requirements for assembling multilayer objects differ from those for single-layer objects.

For building space-filling multilayer objects, one may close-pack DNA double-helical domains onto a square lattice[10] or onto a honeycomb lattice[7] (**Fig. 3a**). On the square lattice, each double-helical domain may have up to four neighbors arranged in fourfold symmetry. On the honeycomb lattice, each double-helical domain may have up to three neighbors arranged in threefold symmetry.

Double-helical domains are constrained to a particular lattice position by antiparallel strand cross-overs along the helical axis that connect to neighboring double-helical domains. The spacing of cross-overs along the helical direction depends on the packing lattice. The cross-over spacing rule for the honeycomb lattice is illustrated in **Figure 3b**. A B-form DNA double-helical domain has a natural helicity of 10.5 bp per full 360° turn[37]. Each strand in the double-helical domain rotates by 240° about the helical axis every 7 bp. When starting at a clock face 'noon' position on a 5′ to 3′ strand in a DNA double-helical domain that is pointing away
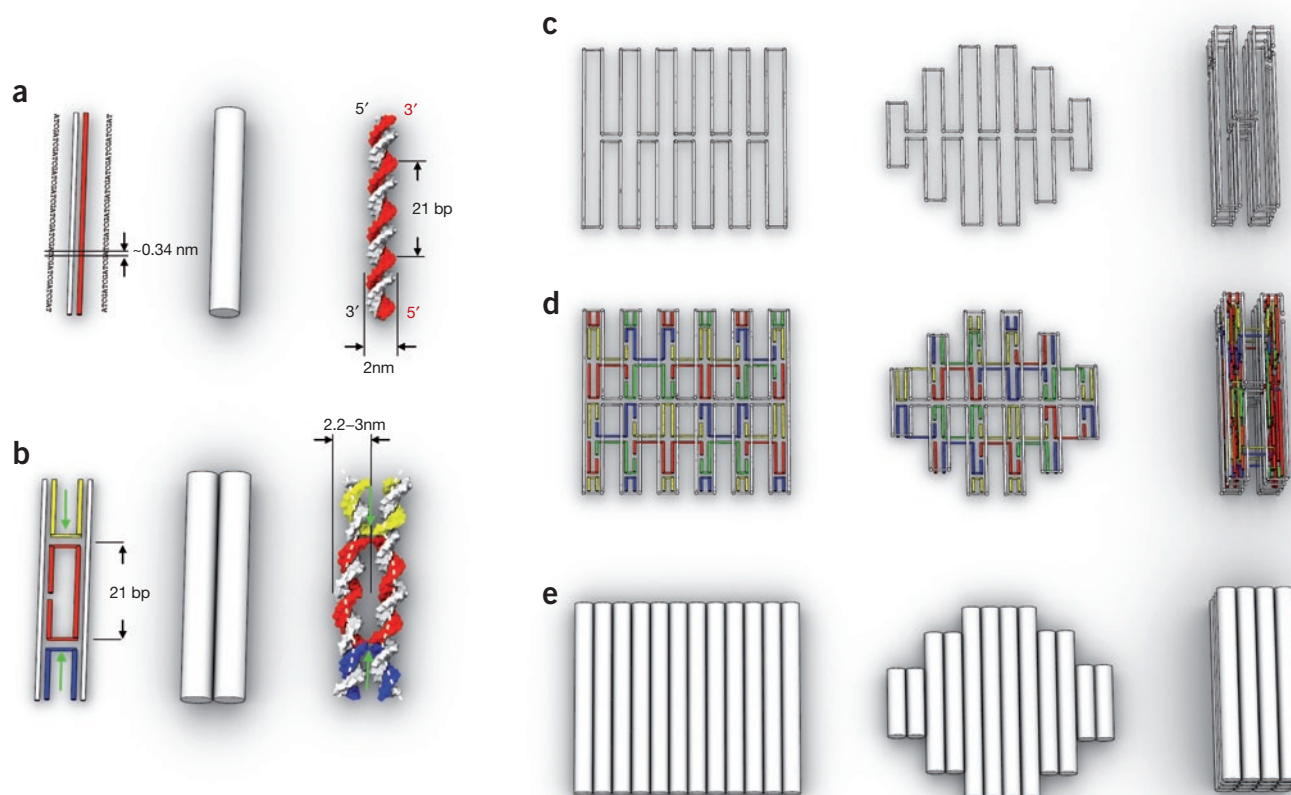
Figure 2 | The scaffolded DNA origami design concept. (**a**) In primitives of scaffolded DNA origami, DNA double helices are represented schematically either as two adjacent lines (left; the white line represents the scaffold strand in white and the staple strand in color) or solid cylinders (middle). A detailed rendering of a B-form double-helical domain is also shown (right). (**b**) Individual DNA double-helical domains may be connected to adjacent double-helical domains by interhelix cross-overs (arrows). The interhelix connections are formed by U-turns of the covalent phosphate backbone of either the staple or scaffold strand. Interhelix connections are depicted schematically as lines perpendicular to the lines that represent helices. In the cylinder representation, cross-overs are not drawn. (**c**) Examples of single- and multilayer scaffold routing solutions through DNA origami object. (**d**) Examples for complete scaffold-staple layouts, with staples colored differently to highlight their individual paths through the structures. (**e**) Single- and multilayer DNA origami objects in cylinder representation.

from the observer, 7 bp downstream the backbone of that strand will be at a position equivalent to 8 p.m., 14 bp downstream will be 4 a.m. the next day and 21 bp downstream it will again correspond to the noon position. To constrain DNA double-helical domains to a honeycomb lattice, one can thus place cross-overs in constant intervals of 7 bp to each of three possible neighboring helical domains with connections between a particular pair of neighboring double-helical domains occurring every 21 bp.

Deviating from the constant 7-bp cross-over spacing rule in honeycomb-lattice packing causes local undertwist or overtwist as well as axial strain[8]. The targeted creation of such local sources of mechanical stress can be incorporated in the design to build objects that have global twist or global bending with tunable curvature (**Fig. 1e–g**)[8].

Close-packing DNA double-helical domains onto a square lattice requires placing cross-overs to four nearest neighbors arranged in fourfold symmetry. Native B-form DNA geometry dictates a constant cross-over spacing of 21 bp between a particular pair of neighboring helical domains (**Fig. 2a,b**). It follows that cross-overs to the remaining three neighbors in the square lattice should be distributed with an average spacing of 21/4 = 5.25 bp. This can only be achieved by making use of nonconstant cross-over spacing intervals.

One elegant way to achieve a square lattice packing with constant cross-over spacing intervals is to assume B-form DNA has an average helicity of 10.67 bp per turn[1,10]. A fourfold symmetry emerges with the backbone of a strand rotating by 270° in intervals of 8 bp. Thus, cross-overs to four neighbors in fourfold symmetry may be placed in intervals of 8 bp, with cross-overs to one of the four neighbors in 32-bp intervals.

A constant 8-bp cross-over spacing in square lattice packing causes underwinding of each of the double-helical domains from the native 10.5 bp to the imposed 10.67 bp per turn, resulting in twisting torques that are transmitted by cross-overs. The superposition of internal torques can cause a global twist deformation of the entire object[8,10]. The global twist for objects in square-lattice packing can be eliminated by departing from a constant 8-bp spacing between cross-overs[10] to achieve effective double-helical twist densities that are closer to the natural 10.5 bp per turn twist density. Elimination of global twist on the square lattice was found for effective double-helical twist densities around 10.4 bp per turn[10]. Global twist in multilayer square lattice objects can also be minimized by creating objects with large torsional stiffness in the helical direction[10].
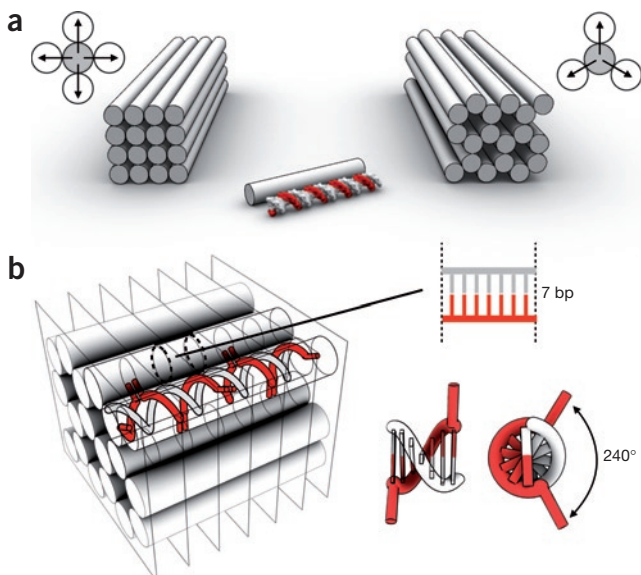
Figure 3 | Packing and cross-over spacing rules for multilayer DNA origami. (**a**) Cross-sectional view of multilayer DNA origami objects in square lattice (left) and honeycomb lattice (right) packing. (**b**) Cross-overs in multilayer objects with honeycomb lattice packing, spaced in constant intervals of 7 bp along the helical axis to link double-helical domains to each of three possible neighbors. The cross-over spacing of 7 bp complies with the natural B-form DNA twist density of 10.5 bp per turn, which corresponds to an average backbone rotation of 240° for a given strand in a DNA double-helical domain.

Single-layer square lattice DNA origami objects with a constant spacing of 16 bp between cross-overs to neighboring double-helical domains likely adopt a twisted shape in solution. Adhesion interactions with surfaces may abolish the twist deformations resulting in objects that lay flat on a surface. For single-layer DNA origami objects twist deformations appear to vanish when surface deposition is achieved by electrostatic immobilization[1,31].

Thus, the square lattice packing rule allows for creating densely packed objects with rectangular features but may require additional effort to eliminate potentially undesired global twist deformations. The honeycomb lattice packing rule by default creates straight albeit more porous structures.

In a DNA origami object both staple and scaffold strands can contribute cross-overs for connecting double-helical domains. To accommodate both scaffold and staple cross-overs one can define two cross-over reference frames that are shifted in the helical direction by 5 bp or 6 bp (corresponding to a backbone rotation of ~180°). This approach neglects the major and minor groove in B-form DNA but appears not to cause global shape deformations for multilayer objects with sufficient thickness (≥3 layers) or cross-sectional aspect ratio close to 1. For thinner objects it may be critical to keep track of major and minor groove phosphate position to avoid unwanted rolling up[38]. An alternative is to work with high densities of staple cross-overs and avoid scaffold cross-overs as much as possible.

Finally, to estimate the dimensions of a DNA origami object one may use the following rules of thumb. The length of double-helical domains may be estimated via $N \times 0.34$ nm in which N indicates the number of base pairs in the double-helical domain. The value of 0.34 nm per bp holds true for single-layer square lattice[1] and for multilayer honeycomb lattice objects[8]. The effective width of a square lattice object along the vertical or horizontal cross-sectional axis (**Fig. 3a**) can be estimated as $2H + (H-1)g$ in which H is the number of 2-nm-wide double-helical domains along that axis and g is the interhelical gap size in nanometers between cross-overs along the same axis[1]. The effective contribution of a single double-helical domain to the cross-sectional dimensions of multilayer honeycomb lattice objects has been found to range from 2.1 nm to 2.4 nm (refs. 7,8).

Computer-aided engineering for DNA origami

Computational tools for predicting 3D structure of DNA origami designs before initiating cost-intensive staple oligonucleotide synthesis are currently lacking. Such tools would be of particular value in designing complex objects that incorporate curved and twisted elements. To this end we developed the computational tool named computer-aided engineering for DNA origami (CanDo) that uses the finite element method to compute 3D DNA origami shapes based on caDNAno design files (**Fig. 4**). CanDo models base pairs as two-node beam finite elements that represent an elastic rod with effective geometric (length of 0.34 nm and diameter of 2.25 nm; ref. 8) and material (stretch modulus of 1,100 pN, bend modulus of 230 pN nm^2 and twist modulus of 460 pN nm; refs. 2,39) parameters. Sequence details are neglected at present, and users may specify custom geometric and mechanical parameters for double-helical DNA domains. Each finite element node has three translational degrees of freedom for the center position of the cross-section and three rotational degrees of freedom for the orientation of the cross-section in torsion and bending[40]. Strand cross-overs defined in the caDNAno design file are modeled as rigid constraints that connect end nodes of base pairs that are coupled by interhelical cross-overs. To compute the 3D structure, CanDo first creates an initial configuration in which all double helices defined in the caDNAno source file are arranged linearly in space. This initial configuration is identical to the structure shown in one of the three design panels in caDNAno. CanDo then applies external forces to deform adjacent helices so that rigid cross-overs may be placed between helices based on the connectivity defined in the caDNAno design file. Subsequent release of these external forces followed by structural relaxation using nonlinear finite element analysis leads to deformation and internal strain whenever the connectivity imposed by cross-overs is not compatible with the default geometry of B-form DNA. CanDo performs the numerical analysis using the commercially available finite element analysis software ADINA (automatic, dynamic, incremental linear analysis; Adina R&D). More information about CanDo is available in **Supplementary Note 2**.

caDNAno design files may be submitted for analysis at (http://cando.dna-origami.org/). Users obtain the deformed shape of the relaxed structure as well as heatmaps of the local magnitude of thermally induced fluctuations, which indicate flexibility of the deformed structure. All output is provided in the .bild data format, which can be visualized using freely available 3D viewers such as University of California San Francisco Chimera[41] (http://www.cgl.ucsf.edu/chimera/).

CanDo currently does not model interhelical electrostatic repulsion and neglects major and minor groove details. We will address these features and the capability to model wireframe or tensegrity-like structures in a future version that is currently

under development. However, CanDo does already provide valuable structural feedback, in particular for designs that have considerable curvature and/or twist (**Fig. 4**). Use of caDNAno and CanDo in an iterative manner of design and analysis should lower the barrier to the design of sophisticated DNA origami shapes.

Exploring DNA origami object stability

One may speculate that folded DNA origami objects will remain folded under conditions that leave DNA double-helical domains and the connecting cross-overs intact. We monitored the structural integrity of three test multilayer objects with honeycomb lattice packing (**Fig. 5a,b** and **Supplementary Figs. 2–4**) when we subjected them to elevated temperatures, DNA nucleases, high- and low-salt conditions, acidic conditions and crowding agents. The average staple oligonucleotide length in the three different objects was 41 (18-helix bundle), 42 (24-helix bundle) and 35 (32-helix bundle) nucleotides. We note that results may only be representative for objects built with similar specifications as the test objects.

To explore the thermal stability of the test objects, we heated the samples and monitored the temperature-dependent content of double-stranded DNA by collecting the fluorescence intensity of a reporter dye (**Fig. 5c** and **Supplementary Methods**). We observed melting transitions between 55 °C and 65 °C, ~10 °C below the average melting temperature calculated for each individual staple oligonucleotide sequence used in the designs using mfold[42]. The reduced melting temperatures of the DNA origami objects may be due to destabilizing factors such as electrostatic repulsion between neighboring helices, mechanical strain induced by interhelix cross-overs and entropic cost associated with scaffold looping. We correlated the melting profiles with agarose gel electrophoresis and transmission electron microscopy (TEM) imaging. Typical micrographs of heated objects are shown in **Figure 5d**. Samples incubated at 37 °C appeared identical to the samples stored at room temperature (20 °C) for all test structures. After incubating one of the objects (24-helix bundle)

at 37 °C for 7 d, we did not detect structural changes. But the test objects exhibited partial damage nucleated at the helical interfaces when heated to 55 °C. These observations are consistent with the melting profiles we obtained (**Fig. 5c**) that suggest that the DNA origami objects are not undergoing substantial melting transitions at temperatures up to 50 °C. We conclude that DNA origami objects built with similar average staple length and crossover density as the three test objects can be safely incubated at 37 °C, which is relevant for many cell-culture applications.

We also tested the effect of different solution conditions by incubating the purified test objects overnight at room temperature in (i) cell culture medium (0.5× Dulbecco's modified Eagle medium), (ii) Tris buffer solution containing crowding agents such as 50 mg ml^{-1} bovine serum albumin (BSA) and 50 mg ml^{-1} dextran or containing 1 mol l^{-1} sodium chloride and/or 1 mol l^{-1} magnesium chloride and (iii) buffer titrated to pH 2 by using hydrochloric acid. We did not observe structural alterations as judged by band appearance in agarose gel electrophoresis and/or imaging by TEM in any of these conditions.

Finally, we treated the test objects with nucleases including DNase I, T7 endonuclease I, T7 exonuclease, *Escherichia coli* exonuclease I, lambda exonuclease and MseI restriction endonuclease (**Supplementary Methods**)[43–48]. DNase I and T7 endonuclease I degraded the test objects, but treatment with the other enzymes did not result in structural alterations as judged by direct imaging using TEM and by gel electrophoresis (**Fig. 5e,f**). We studied the kinetics of digestion by DNase I and found that it takes one unit of DNase I about 60 min to degrade 2 ng of our test structures in a 20-μl reaction at 37 °C (**Fig. 5g**). By contrast, one unit of DNase I completely degraded 65 ng of duplex plasmid DNA (pET24b) in a 20-μl volume in less than 5 min (**Fig. 5g**). Unlike plasmid DNA, which is fully exposed to the degrading enzymes, DNA origami objects are shielded because of the close-packed double-helical domains in the structure. Resistance to endo- and exonucleases opens up interesting prospects for the use of multilayer DNA origami objects as encapsulation agents.

Figure 4 | CanDo. (**a–c**) caDNAno design diagram for multilayer DNA origami objects in honeycomb lattice packing with deviations from the constant 7-bp cross-over spacing rule (left). Base-pair insertions and deletions are depicted as loops and crosses, respectively. CanDo 3D structure and local flexibility prediction shown as a heatmap that indicates local root-mean-square fluctuations (RMSFs) (middle). Representative negative-stain TEM micrographs (right). Scale bars, 20 nm. The objects shown in **a** and **b** form circular gears upon multimerization as described elsewhere[8]. The object shown in **c** was made for this work; note the asymmetry in RMSF between the two 'shoulders' of the object, which can be mapped to an asymmetric distribution of cross-overs in the object design. (**d**) CanDo 3D structure and flexibility prediction for a caDNAno design of a tetrameric 60-helix bundle object in honeycomb lattice packing in which insertions are used to create an effective underwinding to 11 bp per turn for each double-helical domain in the object. The caDNAno design file is provided in **Supplementary Figure 5**. CanDo predicts handedness correctly and reproduces within 15% error the extent of global twist deformation as quantified by direct TEM imaging[8]. Typical TEM data for the twisted ribbon is shown in **Fig. 1e**. Rendering of a 50 bp long B-form DNA double helix is included as a length reference (50 bp = 17 nm).
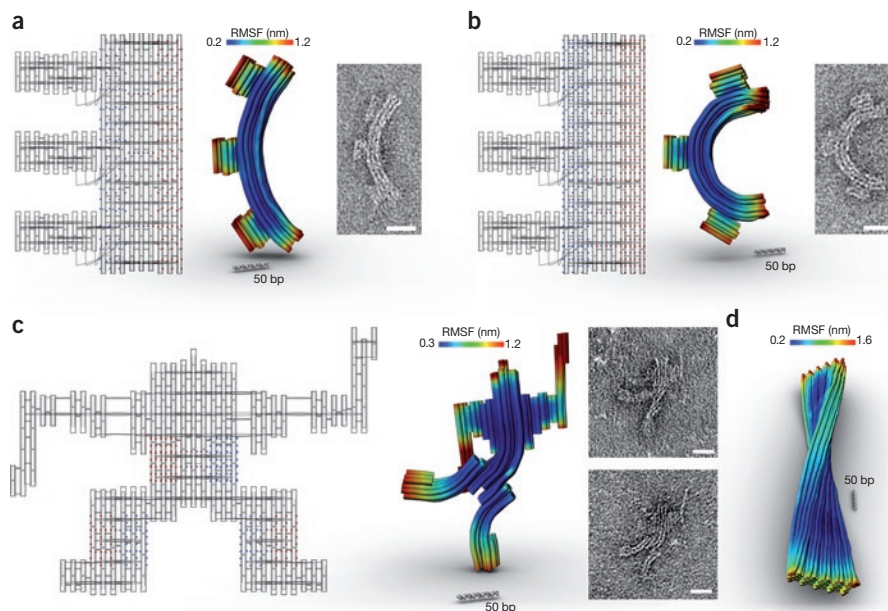
Figure 5 | Thermal stability and resistance against nucleases of three multilayer scaffolded DNA origami test structures. (**a**) Cylinder models of three multilayer DNA origami objects in honeycomb packing used for the stability screens. The object lengths are 140 nm (18-helix bundle), 100 nm (24-helix bundle) and 70 nm (32-helix bundle). The cross-section of a 400-nm-long six-helix bundle was also subjected to melting experiments. (**b**) Representative negative-stain TEM micrographs of the three test origami objects. Scale bars, 20 nm. (**c**) Melting profiles for a 6-, 18-, 24- and 32-helix bundles, and for a 20-nucleotide DNA duplex of sequence 5′-ATTCATATGGTTTACCAGCG-3′. (**d**) Representative single-particle negative-stain TEM micrographs taken after incubating the objects for 2 h at 37 °C, 55 °C and 65 °C. Scale bars, 20 nm. (**e**) Representative single-particle negative-stain TEM micrographs taken after incubating an 18-helix bundle (left), 24-helix bundle (middle) and 32-helix bundle (right) with 10 units (U) of T7 endonuclease I and 1 U of DNase I as indicated. (**f**) Photograph of a UV-irradiated ethidium bromide–stained 2% agarose gel run after incubating purified 32-helix bundles with exo- and endonucleases (10 U each) at 37 °C for 1 h. (**g**) Photograph of a UV-light-irradiated ethidium bromide–stained 2% agarose gel after incubating 2 ng of a 24-helix bundle (left) and 65 ng of a conventional double-stranded DNA plasmid (pET24b, right) with DNase I for indicated amounts of time.
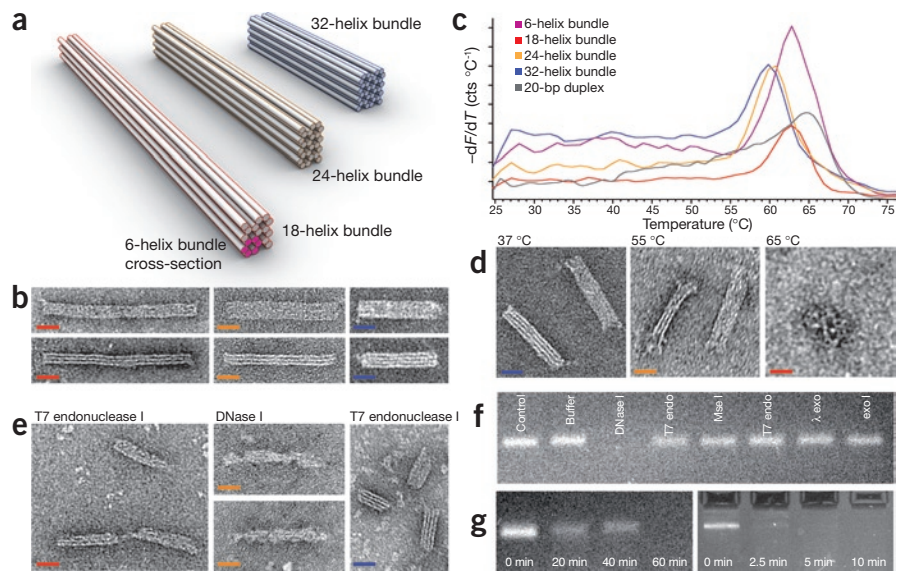
Step-by-step guide to object design and production

The workflow for building DNA origami objects is illustrated in **Figure 6**. We describe how to accomplish each step for an example object shaped like a robot.

Step 1: conceive target shape. The workflow starts with conceiving a target shape that meets certain functional requirements. In light of the intended application one should decide on a single-layer or multilayer structure and whether the object will be built using square lattice or honeycomb lattice packing. Here we decided to build a 75-nm-tall sculpture of a robot using multilayer honeycomb lattice packing (**Fig. 6**). DNA origami offers the opportunity to divide the object into structural modules that can be built and modified separately. To illustrate this idea, we divided the 'robot' into three modules: body, arms and legs.

Step 2: design layout, evaluate design and determine staple sequences. Designing the internal DNA origami scaffold-staple layout for single- and multilayer DNA origami objects using honeycomb lattice or square lattice packing can be accomplished with caDNAno in a matter of a few hours, depending on the complexity of the target structure. Other software packages such as SARSE[4] can help designing single-layer DNA origami objects in square lattice packing. The computational framework CanDo can be used to predict the 3D object structure. This is particularly useful when designing shapes that include curved or twisted structural elements.

We made the scaffold-staple layout for the 'robot' object with caDNAno (**Fig. 6** and **Supplementary Fig. 1**). To highlight structural modularity, we colored groups of staples that form different 'body parts' of the robot object (**Fig. 6**).

In practice, multiple scaffold-staple layouts may have to be made for the same target object to identify a solution that yields well-folded objects. Certain applications will require the site-directed attachment of nanoparticles, proteins or fluorescent dyes. The attachment

chemistry may demand solvent-exposed 5′ or 3′ ends of staple oligonucleotides at particular positions in the object. Such aspects need also be considered when working out the scaffold-staple layout.

Step 3: prepare scaffold DNA and synthesize staples. The quality of folding of DNA origami objects may depend on the scaffold sequence[7] and the particular cyclic permutation used in the design. The single-stranded M13mp18 bacteriophage genome works well as a template for scaffolded DNA origami. A protocol for growing and collecting phage plus purifying the M13mp18 genomic DNA[3] is available as **Supplementary Protocol 1**. Single-stranded scaffold DNA may also be prepared by enzymatic digestion of one strand in double-stranded plasmid DNA[7] or by separation of PCR amplicons[11]. Double-stranded sources of single-stranded scaffold can also be used[49]. Single-stranded scaffold DNA can be purchased from vendors such as New England Biolabs or Bayou Biolabs. We built the robot object with a previously described 8,064-base M13mp18-derived scaffold DNA[7]. We purified it from phage cultures and stored the scaffold DNA at –20 °C at 100 nM concentration in 5 mM Tris base and 1 mM EDTA at pH 8.

DNA origami objects typically integrate a few hundred different staple molecules. A single copy of our robot object required 199 staple molecules in addition to the scaffold molecule. Many commercial vendors offer chemical synthesis of oligonucleotides in multiwell plates, including purification to remove truncated synthesis products.

DNA origami objects are assembled with, on the average, 40-nucleotide-long staple molecules; individual staples may range in length from 18 nucleotides to 50 nucleotides. The lower limit is justified by considering that the binding of staples shorter than 18 nucleotides may not be stable at room temperature. Cost considerations for high-throughput synthesis of sufficiently pure staples typically set the upper length limit to 50 nucleotides. The relationship between staple lengths and DNA origami object stability and folding quality deserves further study. Oligonucleotide synthesis is

typically offered with purification steps such as desalting (retains all truncated synthesis products), reverse-phase cartridge purification (vendors use different names for this process that removes truncated products to a certain extent), high-pressure liquid chromatography and polyacrylamide gel electrophoresis. Staples carrying critical modifications should be obtained with highest possible purity, but DNA origami works well with lower-purity staples (desalted or reverse-phase cartridge purified) that are used in stoichiometric excess over scaffold during assembly reactions.

Staples should be grouped in multiwell plates according to structural modules. For the robot object, we obtained staples in three 96-well plates. Staples forming the different parts of the object were distributed in a compact fashion on the multiwell plates (**Fig. 6**).

Step 4: pool subsets of concentration-normalized oligonucleotides. Equal amounts of concentration-normalized staple oligonucleotides belonging to a structural module are mixed to form a common pool. For the robot object, we prepared three pools that contain the staples forming the body, arms or legs. It is necessary to keep track of the number of different staples that go into each pool to combine the staple pools in volumetric ratios to form combined pools. For the robot object, combined pools could comprise all staples in the design or subsets forming, for example, only body and arms or body, legs and a second set of arm staples with fluorescent dyes. By default, the combined pools are prepared such that each staple is present at the same standard concentration of, for example, 500 nM.

Step 5: run molecular self-assembly reactions. The scaffold-staple layout specifies a structural solution for the mixture of scaffold DNA and staple molecules that minimizes energy through Watson-Crick base-pairing. Whether the target structure corresponds to a global energy minimum of the system depends on solvent conditions and design decisions taken in step 2. Electrostatic repulsion between close-packed double-helical domains at low salt concentrations and internal stresses arising from geometrically incompatible scaffold or staple routing may counteract base-pairing. The goal of the assembly reaction is to reach a minimum energy state at conditions where the minimum corresponds to the target structure. A working assembly method is to mix scaffold and staples in a fixed stoichiometry in magnesium-containing aqueous buffer, followed by subjecting the mixture to a thermal denaturation and annealing procedure[1,7].

Single-layer objects self-assemble faster than multilayer objects. The assembly of multilayer objects can proceed along a multitude of pathways that may not necessarily lead to the fully folded target structure but to partially folded dead ends (kinetic traps) in which parts of the structure need to dissolve before assembly can proceed. Single-layer objects can be assembled by briefly heating the mixture of scaffold and staples to 80 °C, followed by annealing at room temperature during a few hours[1]. Multilayer structures have been observed to require annealing over several days[7]. Factors that affect assembly by thermal annealing of multilayer objects in honeycomb lattice packing have been discussed elsewhere[7]. Isothermal chemical denaturation and renaturation is an alternative to thermal annealing[50]. Folding DNA origami objects by sequential addition of staples to scaffold or by tuning the staple length or sequence composition remain unexplored methods by which the user may direct the system along assembly pathways devoid of substantial kinetic folding traps.

A folding reaction contains scaffold DNA, staple DNA, water, pH-stabilizing buffer and additional ions. Scaffold and staple DNA are typically added such that each staple is present in a defined stoichiometry relative to the scaffold in five- to tenfold excess. Different staple-scaffold stoichiometries may need to be tested. The yield of assembly of multilayer objects is sensitive to $MgCl_2$ concentration. The exact $MgCl_2$ requirements may depend on the staple manufacturer likely because of residuals from varying purification protocols. A detailed protocol for setting up folding reactions is available in **Supplementary Protocol 2**.

For the robot object, we prepared a combined staple pool in which all 199 staple oligonucleotides were present each at a 500 nM effective concentration. For the folding reaction, we filled each of eight

Figure 6 | Step-by-step guide through molecular self-assembly with scaffolded DNA origami. Step 1 involves conceiving a target shape for the intended application. Our robot shape was divided into three modules: body (red), arms (blue) and legs (orange). Step 2 covers designing a scaffold-staple layout for the target shape, evaluating the design and determining the set of staple sequences to build the design. Black vertical lines trace the scaffold strand (as in **Fig. 2c,d**), and colored lines indicate the staple paths. In step 3, scaffold DNA is prepared and staple oligonucleotide synthesis (typically in multiwell plates) is performed. Step 4 involves pooling staple oligonucleotides according to structural modules. In step 5 self-assembly reactions are prepared and subjected to a thermal annealing procedure. Step 6 covers an analysis of the overall folding quality by agarose gel electrophoresis, followed by purification of desired species. Shown is an example of increasing folding quality as evidenced by increasing migration speed of DNA origami folding products observed for longer thermal annealing left to right: annealing from 80 °C to 20 °C in 2 h, 5 h, 10 h, 1 d, 5 d and 7 d as well as scaffold without staples as reference). In step 7 purified objects are subjected to single-particle structural analysis. Scale bar, 70 nm.

Step 1: conceive a target shape

Step 2: design scaffold-staple layout, evaluate design and determine staple sequences

Step 3: prepare scaffold DNA and synthesize staple oligonucleotides

Step 4: pool staple oligonucleotides

Step 5: run molecular self-assembly reactions

Step 6: analyze folding quality and purify

Step 7: analyze structural details

PCR tubes with 20 µl of 100 nM scaffold DNA, 40 µl of the combined staple pool, 10 µl of a 10× folding buffer containing 50 mM Tris base, 50 mM NaCl, 10 mM EDTA (pH 8) and 20 µl pure H_2O. Then to each of the eight PCR tubes we added 10 µl of stock solutions containing various concentrations of $MgCl_2$ dissolved in pure water. This resulted in eight folding reactions that each contained scaffold and staples in a 1:10 stoichiometry and had effective Mg^{2+} concentrations from 10 mM to 24 mM Mg^{2+} in 2 mM steps. We subjected the folding reactions to thermal annealing in a conventional thermal cycler (Tetrad system, Bio-Rad; formerly MJ Research) by heating the mixture briefly to 80 °C and cooling it to 60 °C at a rate of 5 min per degree, followed by cooling it from 60 °C to 25 °C at a rate of 300 min per degree. This thermal annealing ramp takes about 7 d.

Step 6: analyze folding quality and purify objects. Analysis of the quality of folding of DNA origami objects and purification of a desired species can be accomplished with agarose gel electrophoresis[7]. Agarose gels and the running buffer should contain magnesium. For multilayer objects it has been found that for a given object, the objects with lowest defect rate as judged by direct imaging by TEM were those that migrate with the highest speed through a 2% agarose gel[7]. Thus, assembly reactions can be optimized by searching for conditions that yield the fastest migrating species. Selected species can be purified from agarose gel slabs by excising the desired bands, followed by crushing the gel slice with a pistil and centrifuging it through a microcolumn filter. The purification typically results in a solution containing ~2–5 nM of the target shape. The yield for agarose gel purification varies with object shape. A protocol for gel electrophoresis and purification is available in **Supplementary Protocol 3**.

Step 7: single-particle based structural analysis. DNA origami objects may be imaged with negative-stain or cryogenic TEM and with atomic force microscopy (AFM). Shape heterogeneity can be assessed on a particle-by-particle basis. Image processing can help to identify systematic structural flaws or to reconstruct 3D models from single-particle TEM data. Negative-stain TEM with 2% uranyl formate as staining agent is a convenient tool for imaging multilayer objects[7–10]. Protocols for setting up negative-stain TEM and AFM experiments (with the protocol for the latter contributed by P. Rothemund, Caltech) are available in **Supplementary Protocols 4** and **5**.

We imaged the 'robot' object with negative-stain TEM. In a typical TEM image (**Fig. 6**), the 'arm' on the left is resting on the 'hip' of the robot object, with this configuration likely mediated by double-helical blunt-end interactions between the 'hip' and the 'hand'. To prevent undesired stacking interactions, single-stranded loops that cap double-helical domains can be used. One can also hardly recognize the 'arm' of the robot that is supposed to point up. This may be due to a folding defect in this region. We performed basic image processing in which multiple particle images were superimposed to yield the average image (**Fig. 6**). The 'body' and the 'legs' appeared folded as planned, but the two 'arms' of the robot object vanished in noise. This may be caused by a higher rate of folding defects in these parts of the structure and/or by a high degree of conformational flexibility (which in regard to the example structure is likely to be the case). A single particle–based structural analysis may be very helpful to troubleshoot structural details of a DNA origami object.

If a shape does not meet structural specifications, different scaffold-staple layouts can be considered, different scaffold permutations may be used to generate an orthogonal set of staple sequences and different reaction conditions may be tested. In case of a satisfying result of the structural analysis, one may move to further processing or direct application. Further processing may consist of assembling multiple DNA origami objects into larger structures[3,7,8,15,18]. In one impressive example, object production has been scaled up to the milligram regime[3].

Conclusion

Many processes in biology rely fundamentally on the relative position and orientation of interacting molecules. It is notoriously difficult to observe, let alone control, the position and orientation of molecules because of their small size and the constant thermal fluctuations that they experience. Because DNA origami provides a route for placing molecules and constraining their fluctuations in user-defined ways, DNA origami objects can not only be used to improve some existing experimental methods in the molecular biosciences but they also open completely new avenues of exploration. Owing to the apparent structural complexity and the many components involved, designing and building custom DNA origami objects may be a considerable barrier for newcomers to the field. But armed with this primer, the accompanying protocols and computational resources such as caDNAno and CanDo, we hope that scientists with no prior training in the field of structural DNA nanotechnology will be able to develop and build DNA origami objects for their specific purposes.

Note: Supplementary information is available on the Nature Methods website.

1. Rothemund, P.W.K. Folding DNA to create nanoscale shapes and patterns. *Nature* **440**, 297–302 (2006).
2. Lulu, Q. *et al.* Analogic China map constructed by DNA. *Chin. Sci. Bull.* **51**, 2973–2976 (2006).
3. Douglas, S.M., Chou, J.J. & Shih, W.M. DNA-nanotube-induced alignment of membrane proteins for NMR structure determination. *Proc. Natl. Acad. Sci. USA* **104**, 6644–6648 (2007).
4. Andersen, E.S. *et al.* DNA origami design of dolphin-shaped structures with flexible tails. *ACS Nano* **2**, 1213–1218 (2008).
5. Ke, Y. *et al.* Scaffolded DNA origami of a DNA tetrahedron molecular container. *Nano Lett.* **9**, 2445–2447 (2009).
6. Andersen, E.S. *et al.* Self-assembly of a nanoscale DNA box with a controllable lid. *Nature* **459**, 73–76 (2009).
7. Douglas, S.M. *et al.* Self-assembly of DNA into nanoscale three-dimensional shapes. *Nature* **459**, 414–418 (2009).
8. Dietz, H., Douglas, S.M. & Shih, W.M. Folding DNA into twisted and curved nanoscale shapes. *Science* **325**, 725–730 (2009).

9. Douglas, S.M. *et al.* Rapid prototyping of 3D DNA-origami shapes with caDNAno. *Nucleic Acids Res.* **37**, 5001–5006 (2009).

10. Ke, Y. *et al.* Multi-layer DNA origami packed on a square lattice. *J. Am. Chem. Soc.* **131**, 15903–15908 (2009).

11. Pound, E., Ashton, J.R., Becerril, H.A. & Woolley, A.T. Polymerase chain reaction based scaffold preparation for the production of thin, branched DNA origami nanostructures of arbitrary sizes. *Nano Lett.* **9**, 4302–4305 (2009).

12. Endo, M., Hidaka, K., Kato, T., Namba, K. & Sugiyama, H. DNA prism structures constructed by folding of multiple rectangular arms. *J. Am. Chem. Soc.* **131**, 15570–15571 (2009).

13. Kuzuya, A. & Komiyama, M. Design and construction of a box-shaped 3D-DNA origami. *Chem. Commun. (Camb.)* **28**, 4182–4184 (2009).

14. Endo, M., Katsuda, Y., Hidaka, K. & Sugiyama, H. Regulation of DNA methylation using different tensions of double strands constructed in a defined DNA nanostructure. *J. Am. Chem. Soc.* **132**, 1592–1597 (2010).

15. Endo, M., Sugita, T., Katsuda, Y., Hidaka, K. & Sugiyama, H. Programmed-assembly system using DNA jigsaw pieces. *Chem. Eur. J.* **16**, 5362–5368 (2010).

16. Liedl, T., Högberg, B., Tytell, J., Ingber, D.E. & Shih, W.M. Self-assembly of three-dimensional prestressed tensegrity structures from DNA. *Nat. Nanotechnol.* **5**, 520–524 (2010).

17. Han, D., Pal, S., Liu, Y. & Yan, H. Folding and cutting DNA into reconfigurable topological nanostructures. *Nat. Nanotechnol.* **5**, 712–717 (2010).

18. Liu, W., Zhong, H., Wang, R. & Seeman, N.C. Crystalline two-dimensional DNA-origami arrays. *Angew. Chem. Int. Edn. Engl.* **50**, 264–267 (2010).

19. Saccà, B. *et al.* Orthogonal protein decoration of DNA origami. *Angew. Chem. Int. Edn. Engl.* **49**, 9378–9383 (2010).

20. Shih, W.M. & Lin, C. Knitting complex weaves with DNA origami. *Curr. Opin. Struct. Biol.* **20**, 276–282 (2010).

21. Nangreave, J., Han, D. & Yan, H. DNA origami: a history and current perspective. *Curr. Opin. Chem. Biol.* **14**, 608–615 (2010).

22. Kershner, R.J. *et al.* Placement and orientation of individual DNA shapes on lithographically patterned surfaces. *Nat. Nanotechnol.* **4**, 557–561 (2009).

23. Sharma, J. *et al.* Toward reliable gold nanoparticle patterning on self-assembled DNA nanoscaffolds. *J. Am. Chem. Soc.* **130**, 7820–7821 (2008).

24. Stearns, L.A. *et al.* Template-directed nucleation and growth of inorganic nanoparticles on DNA scaffolds. *Angew. Chem. Int. Edn. Engl.* **48**, 8494–8496 (2009).

25. Kuzyk, A., Laitinen, K.T. & Törmä, P. DNA origami as a nanoscale template for protein assembly. *Nanotechnology* **20**, 235305 (2009).

26. Shen, W., Zhong, H., Neff, D. & Norton, M.L. NTA directed protein nanopatterning on DNA Origami nanoconstructs. *J. Am. Chem. Soc.* **131**, 6660–6661 (2009).

27. Kuzuya, A. *et al.* Precisely programmed and robust 2D streptavidin nanoarrays by using periodical nanometer-scale wells embedded in DNA origami assembly. *Chembiochem* **10**, 1811–1815 (2009).

28. Bui, H. *et al.* Programmable periodicity of Quantum Dot arrays with DNA origami nanotubes. *Nano Lett.* **10**, 3367–3372 (2010).

29. Pal, S., Deng, S., Ding, B., Yan, H. & Liu, Y. DNA-origami-directed self-assembly of discrete silver-nanoparticle architectures. *Angew. Chem. Int. Edn. Engl.* **15**, 2700–2704 (2010).

30. Hung, A.M. *et al.* Large-area spatially ordered arrays of gold nanoparticles directed by lithographically confined DNA origami. *Nat. Nanotechnol.* **5**, 121–126 (2010).

31. Steinhauer, C., Jungmann, R., Sobey, T.L., Simmel, F.C. & Tinnefeld, P. DNA origami as a nanoscopic ruler for super-resolution microscopy. *Angew. Chem. Int. Edn. Engl.* **48**, 8870–8873 (2009).

32. Voigt, N.V. *et al.* Single-molecule chemical reactions on DNA origami. *Nat. Nanotechnol.* **5**, 200–203 (2010).

33. Maune, H.T. *et al.* Self-assembly of carbon nanotubes into two-dimensional geometries using DNA origami templates. *Nat. Nanotechnol.* **5**, 61–66 (2009).

34. Seeman, N.C. Nucleic acid junctions and lattices. *J. Theor. Biol.* **99**, 237–247 (1982).

35. Fu, T.J. & Seeman, N.C. DNA double-crossover molecules. *Biochemistry* **32**, 3211–3220 (1993).

36. Seeman, N.C. Nanomaterials based on DNA. *Annu. Rev. Biochem.* **79**, 65–87 (2010).

37. Drew, H.R. *et al.* Structure of a B-DNA dodecamer: conformation and dynamics. *Proc. Natl. Acad. Sci. USA* **78**, 2179–2183 (1981).

38. Rothemund, P.W.K. *et al.* Design and characterization of programmable DNA nanotubes. *J. Am. Chem. Soc.* **126**, 16344–16352 (2004).

39. Gore, J. *et al.* DNA overwinds when stretched. *Nature* **442**, 836–839 (2006).

40. Bathe, K.J. *Finite Element Procedures* (Prentice Hall, 1996).

41. Pettersen, E.F. *et al.* UCSF Chimera—a visualization system for exploratory research and analysis. *J. Comput. Chem.* **25**, 1605–1612 (2004).

42. Zuker, M. Mfold web server for nucleic acid folding and hybridization prediction. *Nucleic Acids Res.* **31**, 3406–3415 (2003).

43. Kunitz, M. Crystalline desoxyribonuclease; isolation and general properties; spectrophotometric method for the measurement of desoxyribonuclease activity. *J. Gen. Physiol.* **33**, 349–362 (1950).

44. White, M.F., Giraud-Panis, M.J., Pöhler, J.R. & Lilley, D.M. Recognition and manipulation of branched DNA structure by junction-resolving enzymes. *J. Mol. Biol.* **269**, 647–664 (1997).

45. Kerr, C. & Sadowski, P.D. Gene 6 exonuclease of bacteriophage T7. II. Mechanism of the reaction. *J. Biol. Chem.* **247**, 311–318 (1972).

46. Little, J.W. Lambda exonuclease. *Gene Amplif. Anal.* **2**, 135–145 (1981).

47. Lehman, I.R. & Nussbaum, A.L. The deoxyribonucleases of *Escherischia coli*. V. On the specificity of exonuclease I (phosphodiesterase). *J. Biol. Chem.* **239**, 2628–2636 (1964).

48. Morgan, R.D. Mse I, a unique restriction endonuclease from *Micrococcus* species which recognizes 5′ T decreases TAA 3′. *Nucleic Acids Res.* **16**, 3104 (1988).

49. Högberg, B., Liedl, T. & Shih, W.M. Folding DNA origami from a double-stranded source of scaffold. *J. Am. Chem. Soc.* **9**, 4302–4305 (2009).

50. Jungmann, R., Liedl, T., Sobey, T.L., Shih, W.M. & Simmel, F.C. Isothermal assembly of DNA origami structures using denaturing agents. *J. Am. Chem. Soc.* **130**, 10062–10063 (2008).